MRI Birdcage RF Coil Resonance with Uncertainty and Relative Error Convergence Rates[1]

Jeffrey T. Fong[2*], N. Alan Heckert[3], James J. Filliben[3], Pedro V. Marcal[4], Robert Rainsberger[5], Karl F. Stupic[6], and Stephen E. Russek[6]
1. Contribution of the National Institute of Standards & Technology (NIST). Not subject to copyright.
2. Applied & Computational Mathematics Division, NIST, Gaithersburg, MD 20899-8910, U.S.A.
*Corresponding author contact, *fong@nist.gov*, or, *fong70777@gmail.com*
3. Statistical Engineering Division, NIST, Gaithersburg, MD 20899-8960, U.S.A.
4. MPact Corp., Oak Park, CA 91377, U.S.A.
5. XYZ Scientific Applications, Inc., Pleasant Hill, CA 94523, U.S.A.
6. Applied Physics Division, NIST, Boulder, CO 80301, U.S.A.

Abstract: In a magnetic resonance imaging (MRI) system, it is necessary to excite the nuclei of a patient into coherent precession for imaging. This requires a coupling between the nuclei and a source of radio frequency (RF) power using a transmitter. To receive a meaningful signal, we also need a coupling between the nuclei and an external circuitry known as the receiver. Both the transmitter and the receiver are called RF coils or resonators, and are key components in any MRI system. In this paper, we use COMSOL 5.2a to model a NIST prototype birdcage RF coil using two low-pass coil mesh design types: Mesh-1, a series of 15 all-tetra-10-element designs with degrees of freedom (d.o.f.) ranging from 169,906 (very coarse) to 3,640,696 (very fine), and Mesh-2, a series of 15 mixed-hex-27-and-tetra-10-element designs with d.o.f. ranging from 188,812 (very coarse) to 2,615,980 (very fine). For each of the 30 meshes, we compute its first resonance frequency, f_{res}, and its time average reflection coefficient given by S_{11} in dB unit. After obtaining 15 pairs of the two parameters, (f_{res} , S_{11}), for Mesh-1 and Mesh-2, we use a 4-parameter logistic function nonlinear least squares fit algorithm to obtain an estimate of the two parameters at infinite degrees of freedom (d.o.f.) as well as their uncertainty (*Unc*) at one-billion-d.o.f. and relative error convergence rates (*RECR*). It is interesting to see that the COMSOL analysis results of the two mesh types differ significantly from each other as shown below:

	f_{req} (MHz)	S_{11} (dB)	*Unc* (S_{11}) (%)	*RECR* (S_{11})
Mesh-1 (all-tetra)	19.271	- 3.843	3.27	- 1.43.
Mesh-2 (mixed)	19.365	- 4.237	10.76	- 0.54.

Based on the classical theory of error estimates for finite element method and the general theory of statistical analysis, we conclude that Mesh-1 (all-tetra-10) solution is the more accurate of the two and should be chosen to compare with experimental data.

Keywords: Accuracy assessment metric (AAM), Birdcage RF coil design, computational modeling, COMSOL, DATAPLOT, electromagnetics, element type, FEM, finite element method, hexahedron element, logistic function, magnetic resonance imaging, mesh density, MRI, nonlinear least squares method, relative error convergence rate, resonance frequency, statistical analysis, super-parametric method, tetrahedron element, time-average reflection coefficient, uncertainty quantification.

1. Introduction

In a magnetic resonance imaging (MRI) system, it is necessary to excite the nuclei of a patient into coherent precession for imaging. This requires a coupling between the nuclei and a source of radio frequency (RF) power using a transmitter. To receive a meaningful signal, we also need a coupling between the nuclei and an external circuitry known as the receiver. Both the transmitter and the receiver are called RF coils or resonators, and are key components of an MRI system, and the modeling and prediction of the performance of those coils, with uncertainty quantification, are essential to a successful design and operation of an MRI system (see, e.g., Fig. 1, after Jin [1]).

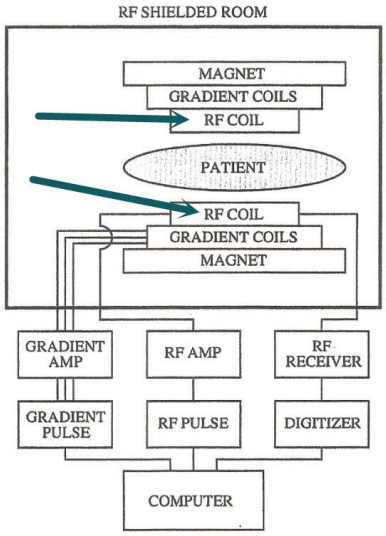

Figure 1. Block diagram of an MRI system [1, p.21].

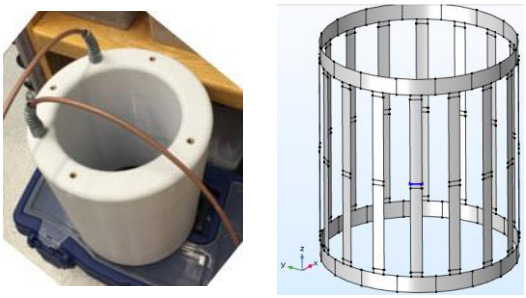

(a) (b)

Figure 2. (a) A NIST prototype 16-leg birdcage RF coil. (b) A partial build of the FEM model of a 16-leg coil.

In a series of papers by Fong, et al. [2-3] on a finite element method (FEM) with uncertainty-based solution of the resonance behavior of a prototype 8-leg birdcage RF coil that was used in the design of an MRI system at the U.S. National Institute of Standards and Technology (NIST) Boulder Laboratory, a software package named COMSOL [4] was applied, along with a nonlinear least squares fit method [3, 5], and a super-parametric method with a design of experiments [2], to address two sources of FEM uncertainty, i.e., the mesh density, and the modeling parameters.

In this paper, we will address the third source of FEM uncertainty, namely, element type, using a more current version of COMSOL [6]. Two mesh designs will be introduced using two different element types: (1) Mesh-1, which will consist of all tetrahedrons of the quadratic type with 10 nodes in each element. (2) Mesh-2, which will consist of a mixture of the quadratic hexahedron-27-node (hex-27) and the tetrahedron-10-node (tetra-10) types. In Section 2, we show the model set-up and the governing equations [7-9] of a prototype 16-leg lowpass birdcage RF coil that was also used in the design of an MRI system at NIST (see Fig. 2).

In Section 3, we show the results of our FEM analysis using COMSOL [6] for two different mesh element designs (see Fig. 3):

Mesh-1: We introduce a series of 15 all-tetra-10-element designs with degrees of freedom (d.o.f.) ranging from 169,906 (very coarse) to 3,640,696 (very fine).

Mesh-2: We introduce a series of 15 mixed-hex-27-and-tetra-10-element designs with d.o.f. ranging from 188,812 (very coarse) to 2,615,980 (very fine).

For each of the 30 meshes, we compute its first resonance frequency, f_{res} , and its time average reflection coefficient given by S_{11} in dB unit. After obtaining 15 pairs of the two parameters, (f_{res} , S_{11}), for each mesh of Mesh-1 and Mesh-2, we use a 4-parameter logistic function nonlinear least squares fit algorithm [3, 5] to obtain an estimate of the two parameters at infinite degrees of freedom as well as their uncertainty (*Unc*) at one-billion-d.o.f., and their relative error convergence rate (*RECR*).

In Section 4, we introduce two posterior metrics, *PM-1* and *PM-2*, for FEM solution accuracy assessment, with *PM-1* based on the solution uncertainty, *Unc* , as estimated at one billion degrees of freedom, and *PM-2* on the relative error convergence rate, *RECR* , as estimated at a range between 10 and 30 millions of degrees of freedom. Using those two metrics, we rank and assess the accuracy of the FEM solutions of the two mesh element types, and choose Mesh-1 the winner.

In Section 5, we add a third metric to the accuracy assessment and again find Mesh-1 to be more accurate than Mesh-2. Some concluding remarks, a list of references, and an acknowledgement section appear in Sections 6, 7, and 8, respectively.

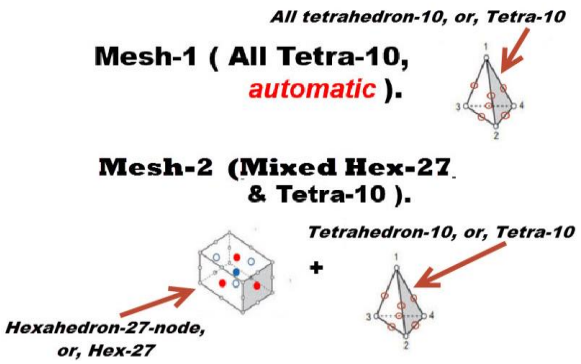

Figure 3. Two designs of FEM meshes of a 16-leg RF coil for a study of FEM uncertainty due to element type.

2. The FEM Model Set-up

In Table 1, we show a partial list of parameters specified in the Mesh-1 design of a 16-leg RF coil, where a special parameter named "refine" is introduced to help us model a series of 15 meshes of increasing mesh density with the d.o.f. varying from 169,906 (refine = 1.0, very coarse) to 3,640,696 (refine = 0.15, very fine). The model includes three material media: copper for the coil, water inside the coil, and air outside. Mesh geometries for Mesh-1 appear in Figs. 4-6, and same for Mesh-2 (mixed element types) in Figs. 7-8. Governing equations solved in COMSOL RF module appear in Fig. 9.

Table 1: Parameters for Mesh-1 design with refine = 0.17.

Name	Expression	Value	Description
Rc	145.6[mm]/2	0.0728 m	Coil radius
Hc	168.6[mm]	0.1686 m	Coil height
w1	12.5[mm]	0.0125 m	Large circular strip width
w2	4[mm]	0.004 m	Small circular strip width
bet1	360/N-bet2	17.5	Large circular strip sector angle
bet2	5	5	Small circular strip sector angle
bet3	6.8	6.8	Short vertical strip sector angle
bet4	6.8	6.8	Long vertical strip sector angle
L3	3.5[mm]	0.0035 m	Short vertical strip length
L4	66.55[mm]	0.06655 m	Long vertical strip length
N	16	16	Number of legs
Ra	1.6*Rc	0.11648 m	Cylinder radius of air domain
Ha	2*Hc*1.1	0.37092 m	Cylinder air height
C	177[pF]	1.77E-10 F	Port capacitance
V0	40[V]	40 V	Excitation voltage
th	0.5[mm]	5E-4 m	Coil thickness
CC	0.001[pF]	1E-15 F	
Rw	0.9*Rc	0.06552 m	Inner water radius
Hw	1.2*Rc	0.20232 m	Inner water height
sig_water	0.1[S/m]	0.1 S/m	Conductivity of water
eps_water	80	80	Water permittivity
f0	20[MHz]	2E7 Hz	Frequency_50
z0	204.1[ohm]	204.1 Ω	Lumped_port_imped_at_fr
fr	19.1[MHz]	1.91E7 Hz	Resonance frequency
f1	18.727[MHz]	1.8727E7 Hz	Lower freq at half z0
f2	19.4145[MHz]	1.9415E7 Hz	Upper freq at half z0
Q	fr/(f2-f1)	27.782	Q-factor
coil_elem_size	8.64[mm]*refine	0.0014688 m	
lam_w	c_const/f0/sqrt(eps_water)/2	0.83795 m	Wave length, water
size_w	(lam_w/nels)*refine	0.02035 m	
lam_a	C_const/f0/2	7.4948 m	Wave length, air
size_a	(lam_a/nels)*refine	0.18202 m	
refine	0.17	0.17	
nels	7	7	

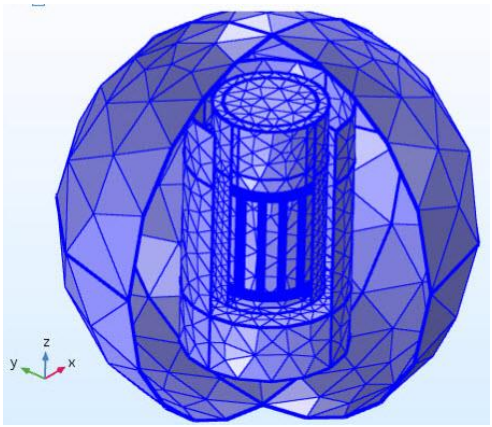

Figure 4. A 3-medium all-tetra (Mesh-1) design.

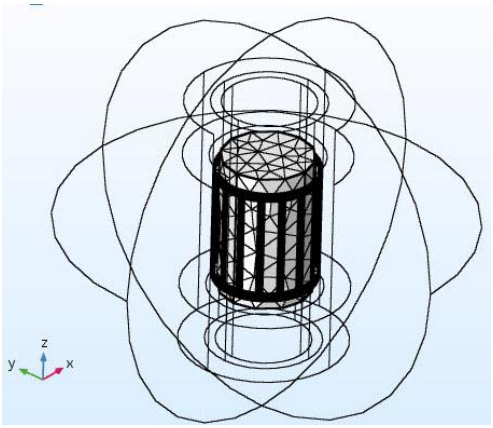

Figure 5. Another view of the all-tetra (Mesh-1) design.

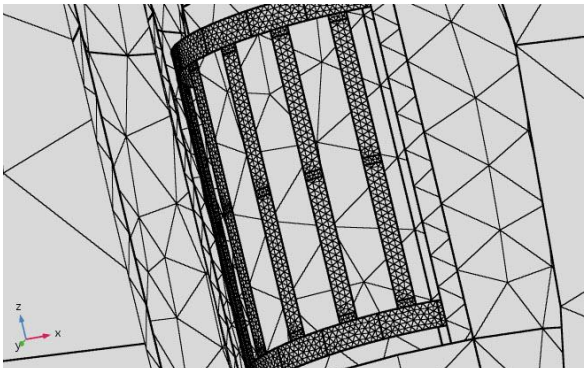

Fig. 6. An enlarged view of the all-tetra (Mesh-1) design.

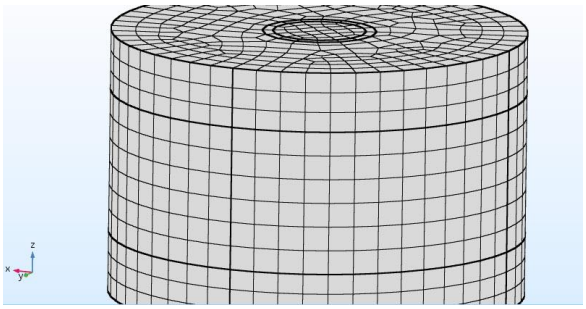

Figure 7. An exterior view of the Mesh-2 design.

.

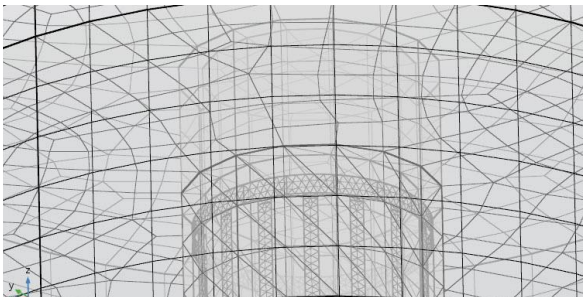

Figure 8. An interior view of the Mesh-2 design.

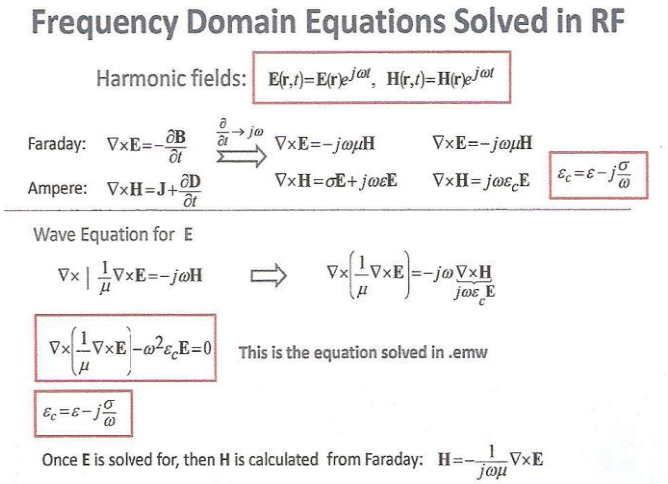

Figure 9.

3. Simulation Results

In Table 2, we show key results of our analysis for 15 meshes of all-tetra-10 (Mesh-1) design listed in increasing d.o.f. from 169,906 (refine = 1.0, very coarse) to 3,640,696 (refine = 0.15, very fine). It is interesting to note that the resonance frequency, f_{res}, varies monotonically from 19.666 MHz (refine = 1.0) to 19.292 MHz (refine = 0.15), a net 1.9 % decrease, whereas the absolute value of the time-average reflection coefficient, S_{11}, ranges eratically from a starting low of 3.959 dB (refine = 1.0) to a high of 4.115 dB (refine = 0.35) and then settles down to a minimum of 3.837 dB (refine = 0.15), a total variation of 6.8 %. The question of interest is: what would be the estimated solution at infinite d.o.f., and how do we know the extrapolated solution is correct?

Table 2: Key Results of FEM Solution for f_{res} and S_{11} based on 15 meshes of all-tetra-10 Mesh-1 design.

Mesh No.	Refine Para-meter	Degree of Freedom	Resonant Frequency (MHz)	S11 (dB)
1	1.00	169,906	19.666	-3.958813
2	0.90	183,408	19.652	-4.060869
3	0.80	199,594	19.652	-3.964955
4	0.70	205,312	19.644	-3.996195
5	0.60	221,120	19.626	-4.026074
6	0.50	284,826	19.597	-4.078074
7	0.40	337,660	19.589	-4.046671
8	0.35	415,914	19.558	-4.114915
9	0.31	805,674	19.447	-4.077531
10	0.24	1,179,720	19.404	-3.9450497
11	0.23	1,416,060	19.369	-4.026016
12	0.21	1,703,198	19.345	-4.000950
13	0.19	2,005,360	19.342	-3.907660
14	0.17	2,849,370	19.299	-3.848283
15	0.15	3,640,696	19.292	-3.837470

Best Estimate using a
4-parameter Logistic Fit = **19.271, - 3.843**

Metric-1: % Uncertainty = **3.3 %.**

Metric-2: Relative Error
Convergence Rate (RECR) = **- 1.43.**

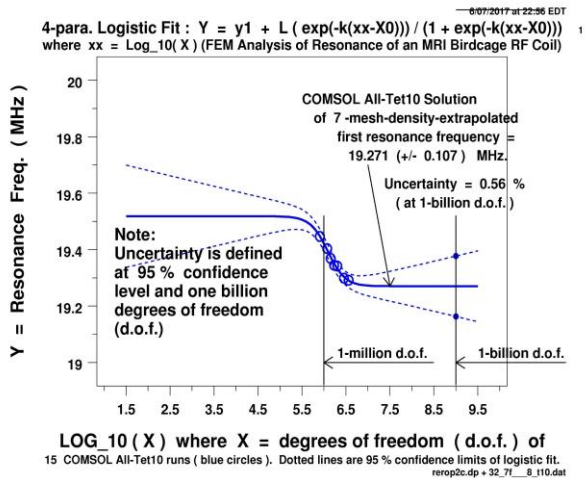

Figure 10. A nonlinear least squares logistic function fit of the resonance freq. of the last seven meshes of Mesh-1.

To anwer this question, we apply the nonlinear least squares logistic function fit approach [3, 5, 10] to the last five to seven meshes of Mesh-1, and obtain, as shown in Figs. 10-11, the estimated f_{res} and $|S_{11}|$ values at infinite d.o.f. to be 19.271 MHz and 3.843 dB, respectively. In the same analysis, we also obtain, as shown in Figs. 11-12, the uncertainty, *Unc* , and the relative error convergence rate, *RECR* , of $|S_{11}|$, as two metrics to be used in Section 4 for accuracy assessment.

In Table 3, we show the same key results of the FEM solution for 15 meshes of Mesh-2. In Fig. 13, we plot the mixed-element-type Mesh-2 analysis result with that of Mesh-1 for accuracy assessment.

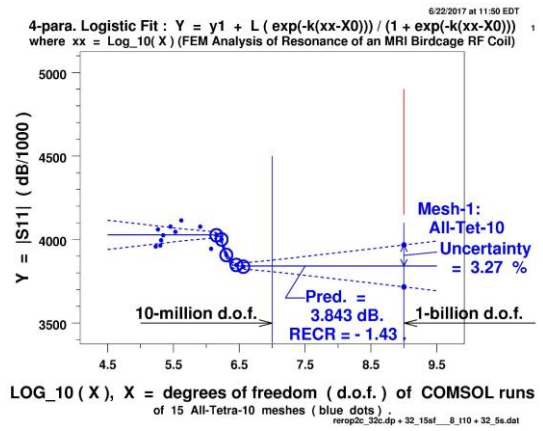

Figure **11.** A nonlinear least squares logistic function fit of absolute value of S_{11} of the last five meshes of Mesh-1.

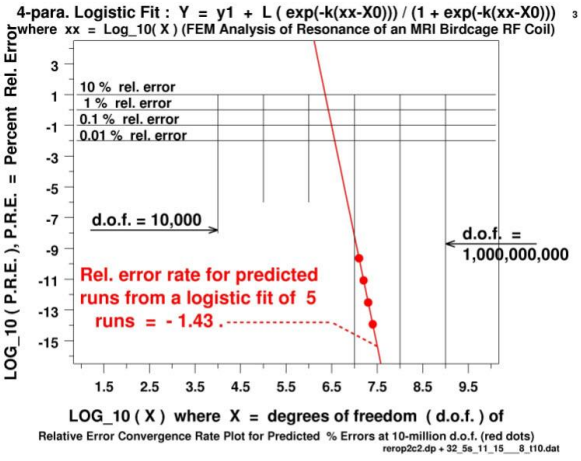

Figure 12. A linear least squares fit of relative error convergence rate, *RECR* , of the predicted values of $|S_{11}|$ at 10 to 30 millions of d.o.f. for Mesh-1 results.

Table 3: Key Results of FEM Solution for f_{res} and S_{11} based on 15 meshes of mixed-element-type Mesh-2 design.

Legend: **H-27 = Hex-27 Type Element.**
T-10 = Tetra-10 Type Element.

Mesh No.	Refine Para-meter	No. of H-27 Elem.	No. of T-10 Elem.	Degree of Freedom	Resonant Frequency (MHz)	S11 (dB)
1	1.00	2,924	13,703	188,812	19.828	- 4.23807
2	0.95	3,292	14,228	203,812	19.801	- 4.29651
3	0.90	3,664	15,683	223,362	19.788	- 4.13724
4	0.85	3,904	17,656	243,182	19.775	- 4.14196
5	0.80	4.754	16,860	262,100	19.756	- 4.21671
6	0.75	4,650	23,544	309,754	19.726	- 4.31801
7	0.70	7,708	24,373	396,044	19.6655	- 4.32680
8	0.65	7,836	24,834	440,528	19.6575	- 4.35539
9	0.60	10,267	31,342	520,506	19.605	- 4.26895
10	0.55	11,848	31,559	566,770	19.58925	- 4.26685
11	0.50	17,346	38,683	764,234	19.544	- 4.26057
12	0.45	22,024	51,146	975,354	19.4904	- 4.25952
13	0.40	30,645	66,002	1,311,222	19.471	- 4.28989
14	0.35	45,353	75,989	1,760,630	19.451	- 4.31001
15	0.30	70.645	104,805	2,615,980	19.401	- 4.20305

Best Estimate via a 4-parameter Logistic Fit = **19.365, - 4.237**

Metric-1: % Uncertainty = **10.8 %**

Metric-2: Rel. Error Convergence Rate (RECR) = **- 0.54.**

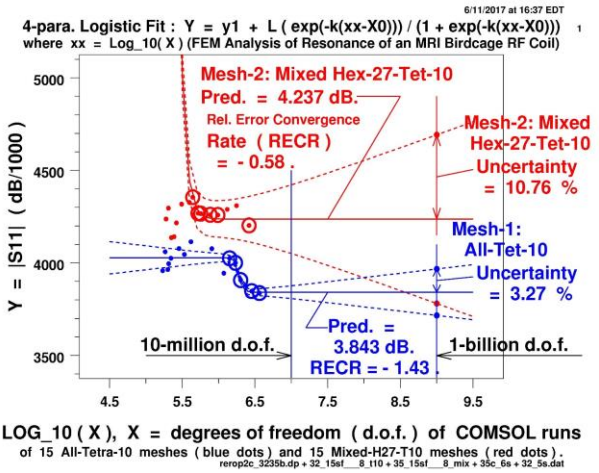

Figure 13. A nonlinear least squares logistic function fit of absolute value of S_{11} of the last five meshes of Mesh-2, superimposed on the same plot for the results of Mesh-1.

4. Two Accuracy Assessment Metrics (AAM)

To assess the correctness of an FEM solution, it is customary for engineers to compute a key quantity of interest at three mesh densities to see if the relative error convergence rate, *RECR*, approaches that predicted by Zienkiewicz and Taylor [11], namely, -0.5 for linear, -0.75 for quadratic, and -1.25 for cubic. Unfortunately, those numbers were estimated from a simple 2-dimensional specialized mesh (Figs. 14-15) and have been shown to be invalid for 3-dimensional meshes in general by Marcal, Fong, Rainsberger, and Ma [10].

In this paper, we introduce two posterior metrics, *PM-1* and *PM-2*, for FEM solution accuracy assessment, with *PM-1* based on the solution uncertainty, *Unc* , as estimated at one billion d.o.f., and *PM-2* on *RECR* , as estimated at a range between 10- and 30-million d.o.f. (see Figs. 16-17). A comparison of Mesh-1 and Mesh-2, as replotted in Fig. 18, shows that Mesh-1 is clearly the winner for less uncertainty and a faster error convergence rate.

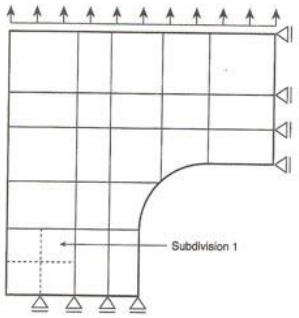

Figure 14. A 2-D mesh (Zienkuewucz & Taylor [11]).

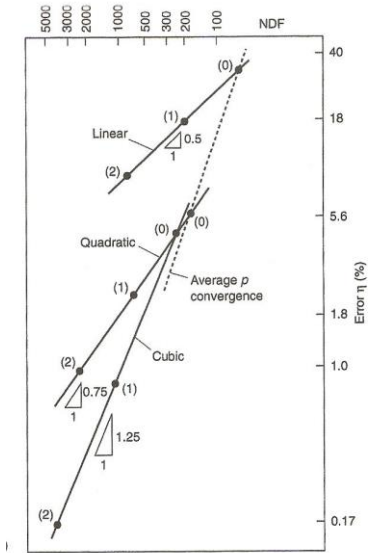

Figure 15. *RECR* (after Zienkuewucz & Taylor [11]).

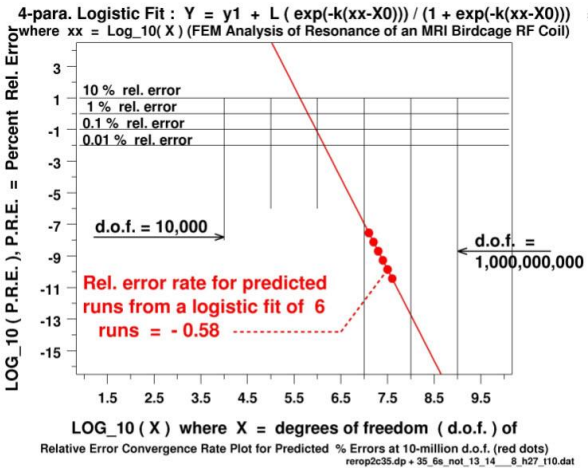

Figure 16. A linear least squares fit of relative error convergence rate, *RECR* , of the predicted values of $|S_{11}|$ at 10 to 30 millions of d.o.f. for Mesh-2 results.

.

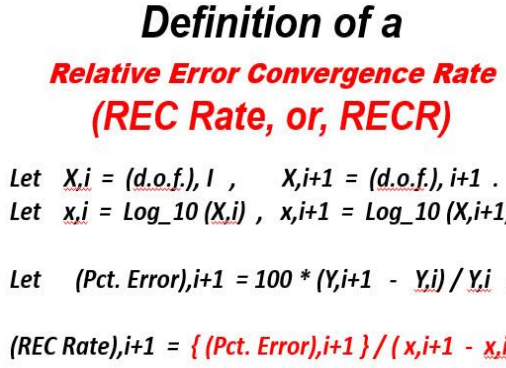

Figure 17. Definition of a relative error convergence rate.

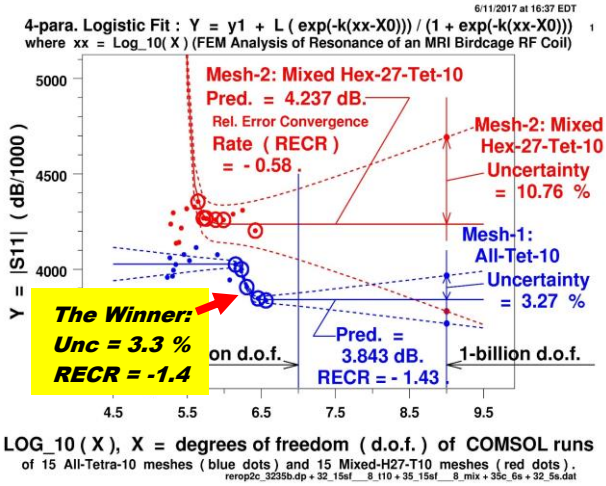

Figure 18. Assessment of the correctness of the absolute value of S_{11} as estimated by the FEM analysis of two sets of meshes of type Mesh-1 (all-tetra) and Mesh-2 (mixed).

5. *A priori* and *Posterior* Metrics for Assessing FEM Solution Accuracy

Both the uncertainty metric, *Unc* , named *PM-1*, and the relative error convergence rate metric, *RECR*, named *PM-2*, are *posterior* in nature, because they can be evaluated only after the FEM solution is completed. In a forthcoming paper by Fong, et al. [12], an *a priori* metric (*AM-1*), defined as the standard error (s.e.) of the Jacobian determinants (*s.e.Jac*) [13] of all the elements in a finite element mesh, is introduced with a smaller *AM-1* indicating a better mesh quality and a more accurate solution. It is interesting to note that, after we applied the third metric, *AM-1*, to the most dense meshes of each of the two mesh types, M-1 and M-2, we again find M-1 the winner as summarized in the following table:

Table 4: Accuracy Assessment using 3 metrics

	PM-1 (Unc)	***PM-2 (RECR)***	***AM-1 (s.e.Jac)***	**Accuracy Assessment**
M-1	**3.3 %**	**- 1.43**	**0.445**	***Winner for being less in all 3 metrics.***
M-2	**10.8 %**	**- 0.54**	**0.554**	

6. Concluding Remarks

We have demonstrated that uncertainty quantification can be achieved in FEM-based solutions when we change mesh density and element type. Based on 3 metrics, one *a priori*, and two *posterior*, and an extrapolation tool using a nonlinear least squares logistic function fit algorithm, it is feasible to rank FEM solutions of the same problem as to which solution is more accurate. This accuracy assessment approach comes with an uncertainty quantification, which is essential for engineering and medical applications where reliability-based decision-making often depends on measurement data and images that inherently contain uncertainty.

7. References

1. Jin, J., *Electromagnetic Analysis and Design in Magnetic Resonance Imaging*. CRC Press, Taylor and Francis Group, New York, NY (1999).
2. Fong, J. T., Heckert, N. A., Filliben, J. J., Ma, L., Stupic, K. F., Keenan, K. E., and Russek, S. E., "A Design of Experiments Approach to FEM Uncertainty Analysis for Optimizing Magnetic Resonance Imaging RF Coil Design," *Proc COMSOL Users' Conference, Oct. 8-10, 2014, Boston, MA, www.comsol.com/ed/direct/conf/conference2014papers/papers/* (2014).
3. Fong, J. T., Heckert, N. A., Filliben, J. J., Marcal, P. V., and Rainsberger, R., "Uncertainty of FEM Solutions Using a Nonlinear Least Squares Fit Method and a Design of Experiments Approach," *Proc COMSOL Users' Conf, Oct. 7-9, 2015, Boston, MA,www.comsol.com/ed/direct/conf/conference2015papers/papers/* (2015).
4. COMSOL, *RF Module User's Guide, Version 4.3, www.comsol.com* (2012).
5. Fong, J. T., Heckert, N. A., Filliben, J. J., Marcal, P. V., Rainsberger, R., and Ma, L. "Uncertainty Quantification of Stresses in a Cracked Pipe Elbow Weldment Using a Logistic Function Fit, a Nonlinear Least Squares Algorithm, and a Super-parametric Method," *Procedia Engineering*, **130**, 135-149 (2015).
6. COMSOL, *RF Module User's Guide, v. 5.2a, www.comsol.com* (2016).
7. Jin, J., *The Finite Element Method in Electromagnetics, 2nd ed.* Wiley (2002).
8. Balanis, C. A., *Antenna Theory: Analysis and Design.* Wiley (2005).
9. Pozar, D. M., *Microwave Enginering, 4th ed.* Wiley (2012).
10. Marcal, P. V., Fong, J. T., Rainsberger, R., and Ma, L., "A High-Accuracy Approach to Finite Element Analysis Using the Hexa 27-node Element," *Proceedings of ASME Pressure Vessels and Piping Conference, PVP-2016, July 17-21, 2016, Vancouver, B.C., Canada,* Paper No. PVP2016-63715, *www,asmeconferences.org/PVP2016* (2016).
11. Zienkiewicz, O. C., and Taylor, R. L., *The Finite Element Method, 5th ed., Vol. 1: "The Basis,"* Sections 8.3 and 8.4, pp. 168-172. Butterworth-Heinemann (2000).
12. Fong, J. T., Marcal, P. V., Rainsberger, R., Heckert, N. A., and Filliben, J. J., " *A priori* and Posterior Metrics for Assessing Accuracy of Finite Element Method-based Solutions using Different Element Types and Densities," to appear in a technical journal.
13. Zienkiewicz, O. C., *The Finite Element Method in Engineering Science, 3rd ed., pp. 190-191.* McGraw-Hill (1977).

8. Acknowledgement

We wish to thank Drs. **Sergei Yushanov**, **Kyle Koppenhoefer**, **Jeffrey Crompton**, all of Altasim Technologies, LLC, Columbus, OH, Dr. **Kathryn Keenan**, **John Koontz**, **Denis Lehane**, Dr. **Li Ma**, and **M. Katherine Pagoaga**, all of NIST, for their assistance during the course of this investigation.